analytical chemistry

Article

Cite This: Anal. Chem. 2018, 90, 5335−5342

pubs.acs.org/ac

Hybrid Surface and Bulk Resonant Acoustics for Concurrent Actuation and Sensing on a Single Microfluidic Device

Emily P. Nguyen,[†] Lillian Lee,[†] Amgad R. Rezk,[†] Ylias M. Sabri,[‡] Suresh K. Bhargava,[‡] and Leslie Y. Yeo*[,†]

[†]Micro/Nanophysics Research Laboratory, School of Engineering, Royal Melbourne Institute of Technology (RMIT University), Melbourne, Victoria 3001, Australia

[‡]Advanced Materials and Industrial Chemistry Group, School of Applied Sciences, Royal Melbourne Institute of Technology (RMIT University), Melbourne, Victoria 3001, Australia

Supporting Information

ABSTRACT: While many microfluidic devices have been developed for sensing and others for actuation, few devices can perform both tasks effectively and simultaneously on the same platform. In piezoelectric sensors and actuators, this is due to the opposing operating requirements for sensing and actuation. Sensing ideally requires narrow resonant peaks characterized by high quality factors, such as those found in quartz crystals. However, these materials usually have poor electromechanical coupling coefficients that are not ideal for actuation. In this work, we show that it is possible to achieve both sensing and actuation simultaneously on a shared device by exploiting the distinct advantages of both bulk waves for effective mass sensing and surface waves for highly efficient microfluidic actuation through a unique hybrid surface and bulk acoustic wave platform. In light of the recent resurgence of interest in portable inhaled insulin devices for personalized diabetes management, we demonstrate the use of this technology for efficient aerosolization of insulin for inhalation without denaturing the protein, while being able to concurrently detect the residual mass of the un-nebulized insulin remaining on the device such that the actual dose delivered to the patient can be determined in real time.

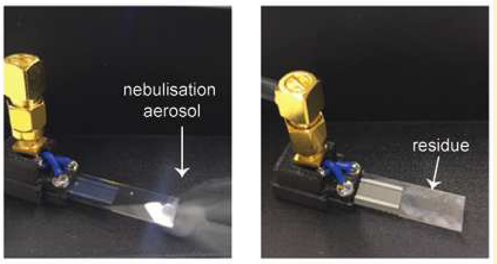

The past two decades have witnessed significant progress in the development of microfluidic actuation and sensing platforms,[1,2] exploiting the latest advances in optics/photonics,[3,4] electrokinetics,[5] and acoustics,[6] in addition to passive mechanisms such as capillary flow and lateral flow immunoassays.[7,8] These capabilities for microfluidic actuation and sensing have nevertheless mainly been developed independent of each other, primarily because of the different operating requirements for actuation and sensing, thus necessitating considerable effort in cross-platform integration to realize a practical multifunctional microfluidic device. While it is often desirable to carry out actuation and sensing on the same platform to facilitate miniaturization and minimize material and manufacturing costs, such ability has largely been elusive to date.

Surface acoustic wave (SAW) platforms are an example where such developments in actuation and sensing have largely taken place independent of each other. Having its origins in telecommunications for applications as resonators, delay lines, and band-pass filters,[9,10] SAWs were subsequently employed for sensing in the 1980s,[11] whereas SAW microfluidic actuation was not widely developed until the early 2000s.[12−16]

The divergent device requirements and characteristics for actuation and sensing have moreover made it difficult to integrate both modalities on the same device. While Rayleigh SAW modes excited predominantly on lithium niobate ($LiNbO_3$) have been reported for humidity[17] and gas[18] sensing, among others, the limitation of these modes, particularly for biosensing, lies in their incompatibility with liquid media, since the longitudinal wave component couples into the liquid, leading to sharp attenuation of the wave over much smaller lengths.[11,19−21] Consequently, other acoustic modes such as shear horizontal surface acoustic waves (SH-SAWs) generated on lithium tantalate ($LiTaO_3$),[22,23] or bulk acoustic waves (BAWs) employing thickness shear modes such as those employed in quartz crystal microbalances (QCM),[11] have predominantly been employed for biosensing. This is in contrast to SAW microfluidic actuation,[21,24−27] in which Rayleigh SAWs have almost exclusively been employed. This is because the viscous attenuation in the liquid—a consequence of the leakage of energy of the out-of-plane component of the acoustic wave into the liquid—is the dominant mechanism by which acoustic streaming in the liquid is generated to drive a host of microfluidic actuation schemes, including droplet/microchannel transport[28−33] and other operations such as micromixing,[34−36] microcentrifugation,[37,38] jetting,[39] and nebulization.[40,41] The same Rayleigh SAW mode has also been employed for generating acoustic radiation forces to effect

Received: January 28, 2018
Accepted: March 7, 2018
Published: April 6, 2018

DOI: 10.1021/acs.analchem.8b00466
Anal. Chem. 2018, 90, 5335−5342

particle patterning, sorting, and manipulation in microchannels.[42−47]

More critically, the necessity for sensors to possess sharp resonance bands—characterized by a high quality factor Q of the piezoelectric crystal—such that they are extremely sensitive to mass loading is in direct contrast to the broad resonance peaks and hence large electromechanical coupling coefficients k_t^2 required for an effective actuator so that the crystal remains in resonance, even with slight shifts in the resonant frequency as a consequence of fluctuations in temperature or mass loading. In other words, it is common that piezoelectric crystals with high Q factors such as quartz ($Q \approx 10\,000$) often possess extremely low k_t^2 values ($k_t^2 \approx 0.001\%$), whereas those that possess k_t^2 values sufficient for driving actuation, such as 128° Y-cut X-propagating (128YX) $LiNbO_3$, do not perform as well for sensing due to their low Q factors ($Q \approx 100$, $k_t^2 \approx 5.3\%$).[48,49]

For these reasons, it is not trivial to design multifunctional devices for concurrent actuation and sensing, thus requiring these tasks to be carried out independently and with multiple devices, each with specific designs for individual tasks. Besides introducing complexities associated with integration as well as fluid handling/transfer between multiple devices, such an arrangement is also not always practically expedient nor effective, particularly if miniaturization of the entire platform is desired.

An example where both actuation and sensing is needed on a single device platform is in portable inhaled macromolecular drug-delivery devices.[50] Such an application is, however, particularly challenging for several reasons. Effective actuation is critical given that significant energy is required for aerosolizing liquids via nebulization. This is compounded by the practical demands of a personalized inhalation device, wherein the platform needs to be sufficiently miniaturized for portable hand-held use while being adequately efficient in terms of its power consumption, such that it can be operated with batteries over reasonable durations. Concomitantly, an important functionality of inhalation devices for drug delivery is the ability to detect the residual mass of the therapeutic agent on the device; that is, the amount of drug that is not nebulized and hence not administered. Unlike injections, in which a known or fixed amount of drug is dispensed, determining the dose that is delivered is particularly crucial in pulmonary administration to avoid patient under- or overdosing. Yet this is often difficult and challenging to measure on a portable chip-scale platform simultaneously during delivery. As such, a device that has sufficient Q to provide adequate sensitivity in its sensing capability is necessary, although a high Q device has the tendency to easily depart from resonance and is hence inadequate to satisfy the demands of a practically operational platform in which robust nebulization performance is sustained over the usage period.

We seek to address this dichotomous quandary by exploiting the separate advantages of both surface acoustic waves (where the acoustic wavelength λ is typically much larger than the substrate thickness h, i.e., $h \ll \lambda$), which have recently been shown to be efficient for driving microfluidic actuation,[21,24−27] and bulk acoustic waves (where the substrate thickness is typically much larger than the acoustic wavelength, i.e., $h \gg \lambda$), which, given their ability to store the majority of the acoustic energy in their structure, have higher Q factors and thus exhibit higher sensitives than their surface counterparts despite their lower resonant frequencies—all on a single chip-scale device. This is achieved through the use of recently discovered hybrid surface and bulk waves in what is known as the HYDRA (hybrid resonant acoustics) platform, which involves matching the substrate thickness to the acoustic wavelength; that is, $h \approx \lambda$.[51] In particular, we show the possibility of nebulizing insulin and concurrently detecting its mass residue in real time as a demonstration of a portable inhalation platform for diabetes management; given its noninvasive nature, this constitutes an attractive alternative to conventional administration routes via subcutaneous or intramuscular injection.[52,53]

MATERIALS AND METHODS

Device Fabrication. The HYDRA device used in this study was fabricated from a 500 μm thick 128° YX $LiNbO_3$ substrate (Roditi Ltd., London, U.K.) on which a 10 nm thick layer of chromium, followed by a 500 nm thick layer of aluminum, was sputtered. Interdigitated transducers (IDTs) with 30 finger pairs that are 100 μm wide with 100 μm spacing, corresponding to a resonant frequency of 10 MHz, were then patterned on the substrate via conventional photolithography and wet etching.

Sensor Validation. The mass-sensing capabilities of the HYDRA device were first validated against a QCM (9 MHz RQCM with gold electrodes; Inficon AG, Bad Ragaz, Switzerland) using 5 nm gold nanoparticles (AuNPs, G1402; Sigma−Aldrich Pty. Ltd., Castle Hill, NSW, Australia) as a mass model. To completely remove the surrounding water phase into which they are originally dispersed, the AuNPs were first resuspended in hexane via a phase-change reaction described elsewhere.[54] Briefly, 1 mL of AuNP, suspended in water, was incubated in 500 μL of dodecanethiol, 10 μL of acetone and 1 mL of hexane; all reagents were acquired from Sigma−Aldrich Pty. Ltd. (Castle Hill, NSW, Australia) unless stated otherwise. Once the AuNPs were transferred into the organic phase, the hexane layer was collected and centrifuged at 9000 rpm for 90 min. The supernatant was then discarded and the AuNPs were washed with more hexane. This process was repeated 3−4 times to ensure the removal of excess dodecanethiol. A 25 μg/mL suspension of AuNP in hexane, determined by atomic absorption spectroscopy (AAS; Agilent Technologies Pty. Ltd., Mulgrave, VIC, Australia), was then reconstituted, from which a fixed standard of 10 μg/mL was prepared by serial dilution for use in the validation procedure; no additional reagents (e.g., buffer solutions) were used. Five microliters (50 ng) of the AuNP suspension was then deposited onto both the HYDRA device and the quartz crystal by drop-casting. In the former, care was taken to ensure that deposition was confined to the sensing area of the device shown in Figure 1a, away from the IDTs to avoid confounding effects in the measurements due to electronic loading. After complete evaporation of the organic solvent in a vacuum desiccator, ensuring a dust- and particulate-free environment, the sensors were allowed to stabilize and the measurements were recorded at room temperature. This procedure was then repeated for successive mass depositions. For mass detection of AuNPs on the HYDRA device, this consisted of exciting the bulk wave resonances on the device by applying a sinusoidal electrical input (0 dBm) at the fundamental harmonic (across a range between 3.4 and 3.6 MHz, depending on the mass loading) and measuring the insertion loss parameters after each deposition and evaporation step with a vector network analyzer (VNA, ZNB4; Rohde & Schwarz GmbH & Co KG, Munich, Germany). The same VNA was also used for QCM measurements to observe the shift in

DOI: 10.1021/acs.analchem.8b00466
Anal. Chem. 2018, 90, 5335−5342

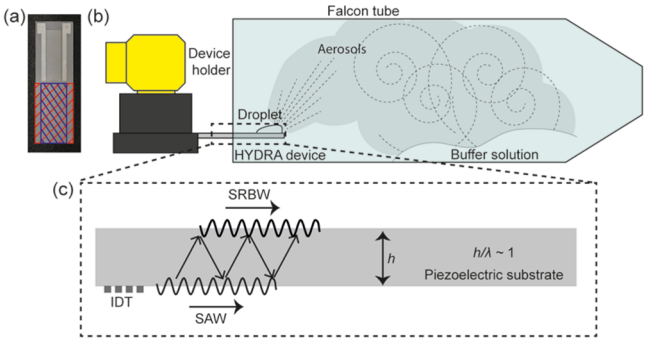

Figure 1. (a) HYDRA device, with bulk mode sensing area hatched in red and SAW mode runway hatched in blue. (b) Schematic depiction of the experimental setup used for concurrent nebulization of insulin and detection of its residual mass on the device. (c) Schematic illustration of the underlying mechanism governing the HYDRA device, in which the substrate thickness h matches the acoustic wavelength λ such that the SAW, generated by the IDTs on the underside of the device (note that the device is inverted in the illustration), is transmitted through the thickness of the substrate and manifests on the opposite face of the device as a surface-reflected bulk wave (SRBW).

resonance from the fundamental harmonic of the crystal at 9 MHz.

Insulin Calibration Standards. Buffer solutions, which typically contain salts to balance or moderate the change in pH and to simulate the requisite physiological environment, are often employed in order for biomolecules to retain their structure and function. As such, we prepared an insulin stock solution in phosphate buffer by diluting human recombinant insulin (91077C; Sigma–Aldrich Pty. Ltd., Castle Hill, NSW, Australia) in mono- and disodium phosphate and 1 mM ethylenediaminetetraacetic acid (EDTA) with an insulin concentration of 3.5 mg/mL (~100 units/mL) typical of commercially available formulations. As the dry mass of the stock solution must encompass the insulin and buffer salts, the overall concentration of the stock solution (i.e., that of buffer salts and insulin) required to yield this concentration was determined by gravimetrically weighing the residue of a 100 μL aliquot of the stock solution after complete evaporation of water. This was found to be 22 mg/mL, of which insulin comprised approximately 16%, or 3.5 mg/mL. Calibration curves for the HYDRA device were then constructed by depositing standard concentrations (through serial dilution) onto the HYDRA device (Figure 1a), evaporating off the solvent in the desiccator, and measuring the insertion loss parameters on the VNA.

Insulin Nebulization and Residue Detection. Various aliquots (10, 20, 50, 75, and 100 μL) of 3.5 mg/mL insulin stock solution were deposited on the working area of the HYDRA device (blue shaded area in Figure 1a) and nebulized by increasing the input power to the device until the insulin solution was completely depleted. The entire nebulization setup was carried out within a Falcon tube as illustrated in Figure 1b, which contained 1 mL of the buffer into which the deposited aerosols were collected. To actuate the nebulization procedure, we drive the device to excite surface resonances at 10 MHz using the same signal generator (N9310A, Agilent Technologies Pty. Ltd., Mulgrave, VIC, Australia) and amplifier (ZHL-5 W-1+, Mini-Circuits, Brooklyn, NY). The nebulization powers were dictated by the amplitude of the input electrical signal, and the power was then measured on an oscilloscope (RTM 1054, Rhode & Schwarz, North Ryde, NSW, Australia), which is given in Table S1. The nebulization rate was calculated by measuring the time over which the initial solution of known volume is completely nebulized, whereas the aerosol size distributions were measured by laser light diffraction (Spraytec, Malvern Instruments, Malvern, U.K.).

The residual mass was subsequently determined through the same sensing procedure described above and reading off the calibration curve. Given that the shift in resonant frequency cannot distinguish between the mass of insulin and that of the precipitated buffer salts that remain on the device, the calibration standard only pertains to the overall residual mass rather than that of the insulin component. In order to quantify the latter, we construct a standard insulin calibration curve. This is done by first placing the device in 1 mL of buffer followed by a brief sonication step to wash off the residue. The actual amount of insulin transferred from the device to the buffer solution is then measured by use of a micro BCA (bicinchoninic acid) protein assay kit (Life Technologies Pty. Ltd., Mulgrave, VIC, Australia), in which the insulin concentration in the solution is determined by absorbance measurements at 562 nm against a standard bovine serum albumin (BSA) calibration curve.

To evaluate the structural integrity of residual and postnebulized insulin, gel electrophoresis was carried out on precast polyacrylamide gels. Briefly, 200 μL of water containing 30 mg of dithiothreitol was mixed with 1 mL of 2× Laemmli buffer solution [4 mL of 10% sodium dodecyl sulfate (SDS), 1.2 mL of 1 M tris(hydroxymethyl)aminomethane (Tris; pH 6.8), 2 mL of glycerol, and 20 μL of bromophenol dissolved in methanol (0.02%)]. Aliquots (25 μL) of this solution were then transferred into PCR tubes containing 4 μL of the collected residual or nebulized insulin, followed by heating to 95 °C for 10 min. Precast polyacrylamide gel electrophoresis (PAGE) cassettes (NuPAGE 4–12% Bis-Tris gels, Life Technologies Pty. Ltd., Mulgrave, VIC, Australia) were prepared as per the manufacturer's specifications and loaded into an electrophoresis tank containing the running buffer [NuPAGE 2-(*N*-morpholino)ethanesulfonic acid (MES) SDS Buffer Kit, Life Technologies Pty. Ltd., Mulgrave, VIC, Australia]. The insulin samples and the protein ladder (Precision Plus Protein Dual Xtra Standards, Bio-Rad Laboratories Pty. Ltd., Gladesville, NSW, Australia) were subsequently loaded into the cassette wells and 100 V of power was applied for 85 min. The gels were finally removed from the cassette and stained (SimplyBlue SafeStain, Life Technologies Pty. Ltd., Mulgrave, VIC, Australia) for an hour, followed by an overnight destaining step with 100 mL of water and 20 mL of 20% salt solution. In addition, we also assessed the residual and postnebulized insulin secondary structure via circular dichroism (CD, 410SF; Aviv Biomedical Inc., Lakewood, NJ).

RESULTS AND DISCUSSION

Validation of the Sensing Platform. Validation of the mass-sensing component of the HYDRA device was accomplished by observing the shift from the absolute resonance frequency of the bulk (Lamb) wave at 3.4645 MHz, Δf, as a consequence of the incremental mass loading Δm upon successive deposition of the AuNPs onto the surface of the device, similar to that observed for the QCM. This is shown in Figure 2. The curve for the QCM closely follows that of the Sauerbrey[55] equation (eq 1)

DOI: 10.1021/acs.analchem.8b00466
Anal. Chem. 2018, 90, 5335–5342

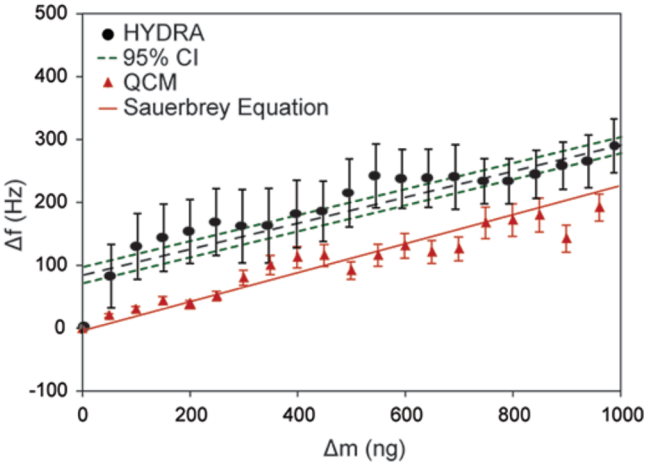

Figure 2. Validation of the mass-sensing capability of HYDRA device against that of the QCM. In both cases, a linear relationship between the shift in resonant frequency Δf and the change in mass loading Δm was observed as AuNPs were incrementally deposited onto the surface of the device. In the case of the QCM, the frequency–mass relationship closely follows that predicted by the Sauerbrey equation (eq 1; solid red line) whereas that of the HYDRA device, which correlates with the resonant frequency associated with the fundamental bulk (Lamb) wave mode at 3.4645 MHz, possesses a different slope. Calibration curves were constructed from an average across three data sets, and the 95% confidence interval (CI) for the HYDRA data set is shown.

$$\Delta f = -\frac{2f_0^{\,2}}{A(\rho_c \mu_c)^{1/2}}\Delta m \tag{1}$$

in which f_0 denotes the resonant frequency and A, ρ_c, and μ_c are the effective area, density, and shear modulus of the crystal, respectively. However, a different slope is obtained with the HYDRA device although it exhibits the same linear relationship between the frequency shift and mass loading. This different slope arises not only due to the different crystal density and shear modulus but also because eq 1 is a solution of the one-dimensional wave equation. While this is appropriate for the wave mode in QCMs and thickness shear mode resonators, in which the entire top surface of the piezoelectric transducer slides horizontally relative to the bottom surface, the bulk (Lamb) wave component in the HYDRA device is strictly two-dimensional, with a pattern resembling that of a checkerboard.[51] More importantly, the excitation of such a wave mode offers a number of advantages for sensing, given that Lamb wave sensors are well-known for their ability to operate at lower frequencies compared to their surface wave counterparts, possess high velocities, facilitate high sensitivity to changes in the mass loading per unit area, and allow the possibility of operation while immersed in liquids,[17] which is a main disadvantage for Rayleigh wave sensors.

Given that the r^2 value was above 96% for validation of the HYDRA device's sensing capability, we then adapted the device for biomolecular detection, in particular for proteins, given our end goal of developing a portable inhalation platform for the delivery of insulin that also allows the delivered dose to be simultaneously measured. The downward shift in the fundamental resonance of the bulk (Lamb) wave mode can be seen in Figure 3a, from which we obtain the insulin calibration standard in Figure 3b, which will subsequently be utilized for detection of the nebulization residual mass.

The linear frequency–mass response and limit of detection (LOD)—calculated from the frequency–mass relationship by the standard 3σ definition—of 390 ng, which is comparable to the 260 ng LOD for the QCM, demonstrates the potential of the HYDRA platform as an effective mass sensor. It is worthwhile recalling at this juncture that the intent is not to acquire a novel sensor with significantly better sensitivity but rather to address a current technological gap by developing a device that is both an effective detection platform that is, at least, comparable to commercially available sensors such as the QCM, as well as an efficient microfluidic actuator. We now turn our attention to demonstrating the possibility of the latter.

Insulin Nebulization. The actuation component of the HYDRA device was conducted by triggering the Rayleigh mode at the resonance frequency, 10 MHz, with varying input power. Figure 4a,b shows the possibility of the device for efficiently generating aerosol droplets of insulin with a mass median aerodynamic diameter of 2.5 μm with a geometric standard deviation of 0.2 μm, which is within the 1–3 μm range necessary for optimal deposition in the alveolar regions in the deep lung;[56] the submicrometer peak can be attributed to the solid protein nanoparticles (on the order of 100 nm) that form when some of the aerosol droplets have completely evaporated.[57] This demonstrates the potential of the HYDRA device for delivering insulin in the form of aerosol droplets that, upon inhalation, have the potential to target the highly vascularized alveolar regions in the respiratory tract to achieve maximum uptake in the bloodstream. At the higher powers (though not the maximum), a nebulization rate of approx-

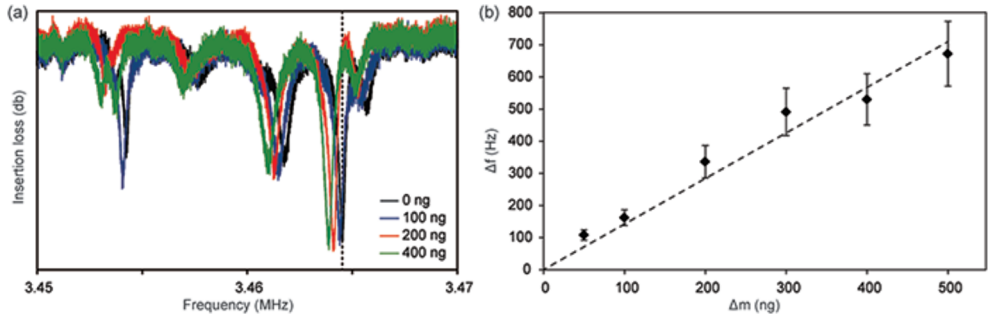

Figure 3. (a) Absolute resonance shift of the fundamental harmonic of the bulk (Lamb) wave mode associated with the HYDRA platform (dashed line) and (b) its frequency–mass response upon deposition of incremental standard amounts of insulin solution, which when evaporated, corresponds to the mass of both insulin and buffer salt on the device. The calibration curve in panel b was constructed from an average across three data sets, and error bars represent the standard error of measurement.

DOI: 10.1021/acs.analchem.8b00466
Anal. Chem. 2018, 90, 5335–5342

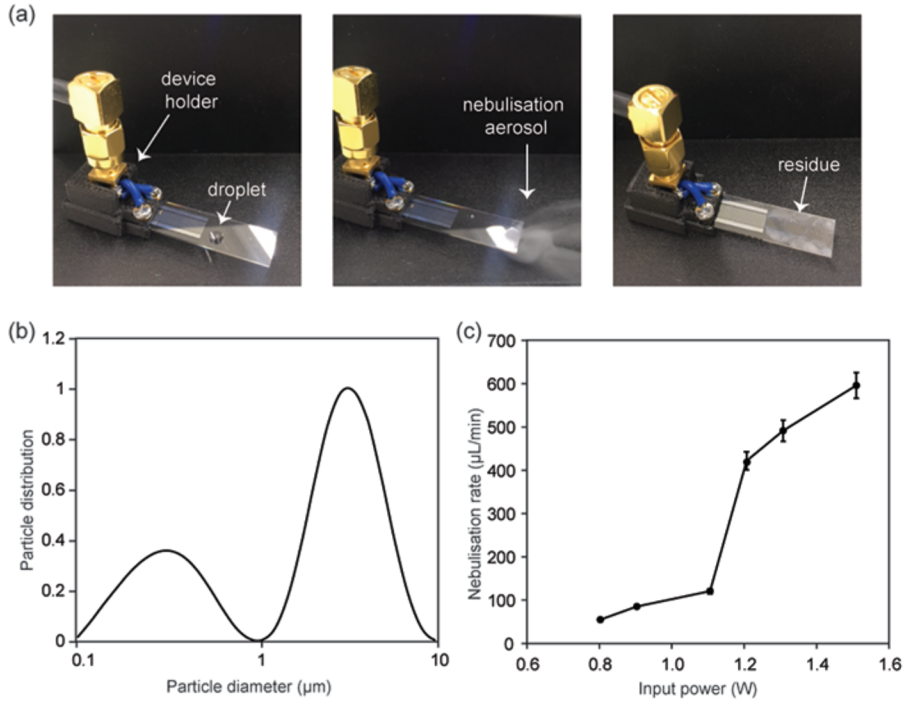

Figure 4. (a) Images showing the aerosolization of an insulin droplet and the residue of un-nebulized insulin left on the surface of the device. To facilitate visualization, this was carried out on a bare device external to the aerosol collection setup in Figure 1b. (b) Size distribution of aerosolized insulin droplets, measured by laser diffraction. (c) Nebulization rate as a function of input power. Error bars represent the standard error of the measurements.

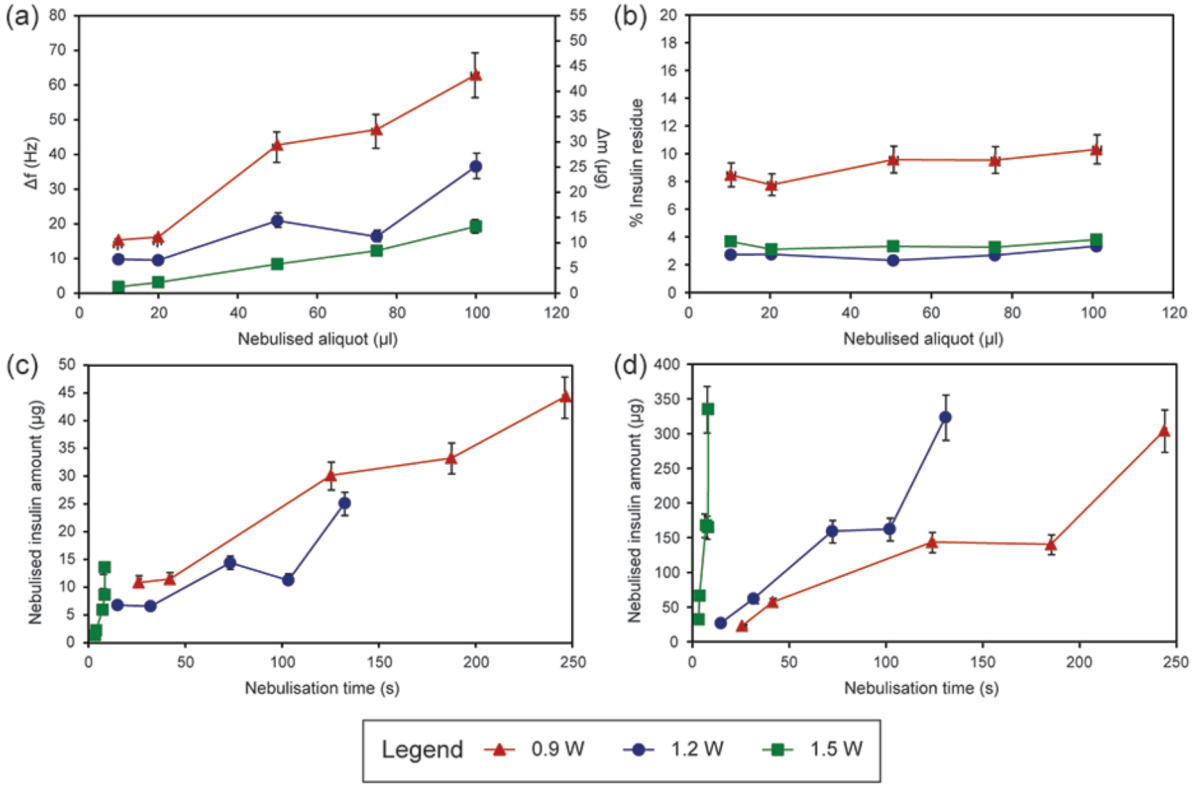

Figure 5. Estimation of the residual mass remaining on the HYDRA device during nebulization. (a) Shift in resonant frequency due to residual mass loading. (b) Percentage of insulin in the residual mass as a function of the amount of insulin stock solution that is nebulized. (c) Actual mass of insulin remaining on the device. (d) Actual amount of insulin (from a total of 0.1 mL of insulin in the initial stock solution) that is nebulized and hence delivered via inhalation as a function of the nebulization time. Error bars represent the standard error of the measurement.

DOI: 10.1021/acs.analchem.8b00466
Anal. Chem. 2018, 90, 5335−5342

imately 600 μL/min can be attained, which is higher than the 400 μL/min typically achieved with vibrating mesh nebulizers.

Further, the chip-scale dimensions of the device and the possibility for battery-powered operation[50] allude to the miniaturizability of the platform for portable, hand-held use, which, together with the low device manufacturing cost (around U.S. $10/device by exploiting the economies of scale associated with mass nanofabrication), constructs a compelling narrative of its potential for personalized inhaled therapeutics. In the case of insulin delivery, such a platform for inhaled therapeutics is motivated by three factors: (1) considerable clinical evidence acquired over a decade of the efficacy of delivering insulin via the pulmonary route,[58−60] with a commercial inhaled insulin product, Afrezza (MannKind Corp., Westlake Village, CA)[61] that has recently been approved by the U.S. Food and Drug Administration;[62,63] (2) there is currently no liquid-based insulin formulation for aerosol delivery [Afrezza and its predecessor, Exubera (Pfizer Inc., New York), are dry powder formulations]; and (3) the potential to increase patient comfort and hence compliance with a noninvasive form of administration, particularly for treating juvenile diabetes.

To demonstrate efficacy of the device as a therapeutic platform and to navigate the appropriate regulatory hurdles for registration of the device, however, it is necessary to show that the nebulization process does not denature the active pharmaceutical ingredient. This is particularly pertinent for biologics such as insulin, given that large molecules are susceptible to denaturation, especially given the large amounts of energy to which they are subjected to during the aerosolization process. Protein unfolding and denaturation is particularly widespread in the majority of nebulizers, either because of the large hydrodynamic shear to which they are subjected, for example, with jet nebulizers, or due to the large pressures associated with the cavitation events responsible for aerosolization in ultrasonic nebulizers.[64] To address this concern, we assess the structural integrity of postnebulized insulin via CD and gel electrophoresis. A comparison between the CD spectra for pre- and postnebulized insulin, as well as the residual drug remaining on the surface of the device, in Figure S1a shows that there is no evidence of structural changes in the protein as a result of the nebulization. Furthermore, the gel electrophoresis results in Figure S1b also show that the nebulization did not result in molecular fragmentation of insulin. That the HYDRA nebulization does not inflict structural damage on macromolecules is consistent with previous results for protein nebulization at high frequencies,[65] given that cavitation is not present at these frequencies and that there is insufficient time to unfold the protein since the molecular shear relaxation times are much longer than the inverse of the period over which the electromechanical field reverses.[64]

Residual Mass Detection. Finally, we demonstrate the concurrent ability of the HYDRA device to function both as an efficient actuator and as an effective sensor; that is, its ability to measure the mass of the residue remaining on the surface of the device together with the nebulization of the insulin solution (Figure 4a). The detection of the residual mass remaining on the surface of the device is carried out in the same manner as that reported above: by comparing the measured shift in the resonance frequency of the fundamental harmonic mode associated with the bulk wave component in the HYDRA device (see, for example, Figure 3a) with the calibration curve in Figure 3b. Figure 5a shows the shift in resonance as the nebulization progresses at input powers of 0.9, 1.2, and 1.5 W (see also Table S2), which, when measured against the standard calibration curve in Figure 3b, allows the residual mass to be ascertained. We note that the shift in resonance frequency due to mass loading is insensitive to the location of the drug on the device, as long as it is within the sensing area and not in contact with the IDTs (Figure 1a); as a precaution to avoid contact with the IDTs, which leads to electrical loading effects, the device can be coated with a thin film of nonconductive material, such as SiO_2.

We note that the results in Figure 5a gives the overall mass of the residue that comprises *both* the insulin as well as the buffer salt that has precipitated from the solution. In order to determine the *actual* amount of insulin that is present in the residue, which is important to estimate the actual amount of insulin that is nebulized and hence administered via inhalation, we measured its concentration by reconstituting the residue in 1 mL of phosphate buffer and running a micro BCA assay on this solution, from which the insulin concentration can be determined via absorbance measurements with a spectrophotometer against a standard BSA calibration curve. The results are shown in Figure 5b, which reports the percentage of insulin in the residue as a function of the amount of insulin solution that is nebulized. We note two important observations as follows: (1) The actual mass of insulin remaining on the device is more or less linearly proportional to the amount of insulin solution that is nebulized. In fact, it is weakly linear and almost invariant. Since the concentration of the initial insulin stock solution is fixed, at 3.5 mg/mL in this case, the amount of insulin remaining on the device that is not delivered is then proportional to the overall residual mass that is measured by the sensor. This is an encouraging finding, as it allows a calibration standard that is valid at least over a fixed concentration range to be obtained, such that it is only necessary to measure the actual amount of insulin via the micro BCA assay to obtain this calibration standard. During actual use of the inhalation platform, it is sufficient for the mass-sensing capability of the device to simply measure the overall residual mass, which can then be correlated to the actual amount of residual insulin by comparison against this calibration standard. It then follows that the dose of insulin delivered can be determined by subtracting this from the amount of insulin in the initial insulin stock solution. (2) The percentage of insulin residue remaining on the device is low, only about 8−11% when the nebulization is carried out at 0.9 W and down to 2−4% at 1.2 and 1.5 W (Figure 5b), corresponding to only roughly ten or a few tens of micrograms over typical administration times (Figure 5c). This is encouraging from the perspective of the efficiency of the device for nebulizing and hence administering the drug via inhalation with little loss and wastage—over 96% of the actual active pharmaceutical ingredient that is nebulized is received by the patient (excluding losses due to deposition of the aerosol droplets in the inhaler body and mouthpiece, which are typically negligible in comparison). That the delivery efficiency increases with increasing input voltage and hence power is also encouraging, given that it is desirable to operate the nebulizer at higher powers to achieve higher nebulization rates (Figure 4c) such that the administration time over which the patient has to inhale is minimized (above 1.1 W, a sharp increase in the nebulization performance is observed, likely because liquid film fragments on the surface of the device that are a consequence of

DOI: 10.1021/acs.analchem.8b00466
Anal. Chem. 2018, 90, 5335−5342

dewetting effects are effectively nebulized). We observe in Figure 5d that the effective insulin delivery rate at 1.5 W, which corresponds to a nebulization rate of 593 μL/min, is 5.9 mg/min. Given that the requisite dose for an average adult of 68 kg is 34 units (0.5 unit kg^{-1} day^{-1}) or 1.19 mg, the dose can be administered in 34 s. This is based on the same concentration as that for the commercial inhaled insulin product Afrezza (MannKind Corp., Westlake Village, CA).[61] Such short inhalation periods under a minute are desirable since a major reason for the low uptake in the use of nebulizers has historically been due to the long inhalation periods (5−15 min) required with conventional technology.

CONCLUSIONS

While a myriad of microdevices, including those driven acoustically, abound to carry out effective sensing or actuation, few, if any, are able to carry out both of these operations concurrently on the same platform. This is because of their contrasting operating requirements. Obtaining high sensitivity necessitates the existence of a sharp resonant peak characteristic of piezoelectric sensing devices with high quality factors. This very same feature, however, means that a departure from resonant operating conditions would lead to a significant decrease in transduction for driving actuation (we thus note that it is unlikely that Lamb wave devices, despite the claim of their superior efficiency for nebulization,[66] would maintain their performance in practice given the propensity for even the slightest of these resonance shifts during operation). Further, piezoelectric materials with high quality factors often do not have large piezoelectric coupling coefficients, and vice versa.

Yet a single platform that can both effectively sense and actuate simultaneously would avoid the need for complex device integration and facilitate ease of miniaturization as well as reduction in materials and manufacturing costs. In this work, we explored one example of a nebulization platform for potential personalized pulmonary drug administration in which the mass sensing capability on the same nebulization device allowed for the delivered dose to be estimated. This capability is expected to facilitate smart device functionality where such information, for example, can provide useful real-time feedback to the patient to avoid medication error and could even be wirelessly transmitted to the patient's practitioner for continuous monitoring—capability that is still largely elusive with current inhaler technology.

ASSOCIATED CONTENT

Supporting Information

The Supporting Information is available free of charge on the ACS Publications website at DOI: 10.1021/acs.analchem.8b00466.

One figure verifying structural integrity of postnebulized insulin by circular dichroic and gel electrophoretic data; two tables summarizing the input power used and the shift in the resonance frequency due to residual insulin mass loading at different input powers and nebulization rates (PDF).

AUTHOR INFORMATION

Corresponding Author

*E-mail leslie.yeo@rmit.edu.au.

ORCID

Suresh K. Bhargava: 0000-0002-9298-5112

Leslie Y. Yeo: 0000-0002-5949-9729

Notes

The authors declare no competing financial interest.

ACKNOWLEDGMENTS

L.L. and A.R.R. are grateful for Vice-Chancellor's postdoctoral fellowships from RMIT University. L.Y.Y. acknowledges support from the Australian Research Council through a Future Fellowship (FT130100672) and through a Discovery Project grant (DP170101061).

REFERENCES

(1) Sackmann, E. K.; Fulton, A. L.; Beebe, D. J. *Nature* **2014**, *507* (7491), 181−189.
(2) Yeo, L. Y.; Chang, H.-C.; Chan, P. P. Y.; Friend, J. R. *Small* **2011**, *7* (1), 12−48.
(3) Psaltis, D.; Quake, S. R.; Yang, C. *Nature* **2006**, *442* (7101), 381−386.
(4) Fan, X.; White, I. M. *Nat. Photonics* **2011**, *5*, 591−597.
(5) Chang, H.; Yeo, L. *Electrokinetically Driven Microfluidics and Nanofluidics*; Cambridge University Press: New York, 2010.
(6) Friend, J.; Yeo, L. Y. *Rev. Mod. Phys.* **2011**, *83* (2), 647−704.
(7) Martinez, A. W.; Phillips, S. T.; Whitesides, G. M.; Carrilho, E. *Anal. Chem.* **2010**, *82* (1), 3−10.
(8) Cate, D. M.; Adkins, J. A.; Mettakoonpitak, J.; Henry, C. S. *Anal. Chem.* **2015**, *87* (1), 19−41.
(9) Campbell, C. K. *Surface Acoustic Wave Devices for Mobile and Wireless Communications*. Academic Press: San Diego, CA, 1998.
(10) Hashimoto, K. *Surface Acoustic Waves in Telecommunications*, 1st ed.; Springer-Verlag: Berlin and Heidelberg, Germany, 2000; DOI: 10.1007/978-3-662-04223-6.
(11) Länge, K.; Rapp, B. E.; Rapp, M. *Anal. Bioanal. Chem.* **2008**, *391* (5), 1509−1519.
(12) Shiokawa, S.; Matsui, Y.; Ueda, T. *Jpn. J. Appl. Phys.* **1990**, *29* (S1), 137.
(13) Kurosawa, M.; Watanabe, T.; Futami, A.; Higuchi, T. *Sens. Actuators, A* **1995**, *50* (1), 69−74.
(14) McHale, G.; Banerjee, M. K.; Newton, M. I.; Krylov, V. V. *Phys. Rev. B: Condens. Matter Mater. Phys.* **1999**, *59* (12), 8262−8270.
(15) Wixforth, A. *Superlattices Microstruct.* **2003**, *33* (5), 389−396.
(16) Guttenberg, Z.; Rathgeber, A.; Keller, S.; Rädler, J. O.; Wixforth, A.; Kostur, M.; Schindler, M.; Talkner, P. *Phys. Rev. E* **2004**, *70* (5), No. 056311.
(17) Sayar Irani, F.; Tunaboylu, B. *Sensors* **2016**, *16* (12), 2024.
(18) Devkota, J.; Ohodnicki, P. R.; Greve, D. W. *Sensors* **2017**, *17* (4), 801.
(19) Rocha-Gaso, M.-I.; March-Iborra, C.; Montoya-Baides, Á.; Arnau-Vives, A. *Sensors* **2009**, *9* (7), 5740.
(20) Calabrese, G. S.; Wohltjen, H.; Roy, M. K. *Anal. Chem.* **1987**, *59* (6), 833−837.
(21) Destgeer, G.; Sung, H. J. *Lab Chip* **2015**, *15* (13), 2722−2738.
(22) Zerrouki, C.; Fourati, N.; Lucas, R.; Vergnaud, J.; Fougnion, J.-M.; Zerrouki, R.; Pernelle, C. *Biosens. Bioelectron.* **2010**, *26* (4), 1759−1762.
(23) Bisoffi, M.; Hjelle, B.; Brown, D. C.; Branch, D. W.; Edwards, T. L.; Brozik, S. M.; Bondu-Hawkins, V. S.; Larson, R. S. *Biosens. Bioelectron.* **2008**, *23* (9), 1397−1403.
(24) Fu, Y. Q.; Luo, J. K.; Du, X. Y.; Flewitt, A. J.; Li, Y.; Markx, G. H.; Walton, A. J.; Milne, W. I. *Sens. Actuators, B* **2010**, *143* (2), 606−619.
(25) Ding, X.; Li, P.; Lin, S.-C. S.; Stratton, Z. S.; Nama, N.; Guo, F.; Slotcavage, D.; Mao, X.; Shi, J.; Costanzo, F.; Huang, T. J. *Lab Chip* **2013**, *13* (18), 3626−3649.
(26) Yeo, L. Y.; Friend, J. R. *Annu. Rev. Fluid Mech.* **2014**, *46* (1), 379−406.
(27) Go, D. B.; Atashbar, M. Z.; Ramshani, Z.; Chang, H.-C. *Anal. Methods* **2017**, *9* (28), 4112−4134.

DOI: 10.1021/acs.analchem.8b00466
Anal. Chem. 2018, 90, 5335−5342

(28) Cecchini, M.; Girardo, S.; Pisignano, D.; Cingolani, R.; Beltram, F. *Appl. Phys. Lett.* **2008**, *92* (10), 104103.
(29) Tan, M. K.; Yeo, L. Y.; Friend, J. R. *EPL* **2009**, *87* (4), 47003.
(30) Schmid, L.; Wixforth, A.; Weitz, D. A.; Franke, T. *Microfluid. Nanofluid.* **2012**, *12* (1), 229−235.
(31) Baudoin, M.; Brunet, P.; Matar, O. B.; Herth, E. *Appl. Phys. Lett.* **2012**, *100* (15), No. 154102.
(32) Dentry, M. B.; Friend, J. R.; Yeo, L. Y. *Lab Chip* **2014**, *14* (4), 750−758.
(33) Collignon, S.; Friend, J.; Yeo, L. *Lab Chip* **2015**, *15* (8), 1942−1951.
(34) Frommelt, T.; Kostur, M.; Wenzel-Schäfer, M.; Talkner, P.; Hänggi, P.; Wixforth, A. *Phys. Rev. Lett.* **2008**, *100* (3), No. 034502.
(35) Shilton, R. J.; Yeo, L. Y.; Friend, J. R. *Sens. Actuators, B* **2011**, *160* (1), 1565−1572.
(36) Jo, M. C.; Guldiken, R. *Microelectron. Eng.* **2014**, *113*, 98−104.
(37) Shilton, R.; Tan, M. K.; Yeo, L. Y.; Friend, J. R. *J. Appl. Phys.* **2008**, *104* (1), 014910.
(38) Destgeer, G.; Cho, H.; Ha, B. H.; Jung, J. H.; Park, J.; Sung, H. J. *Lab Chip* **2016**, *16* (4), 660−667.
(39) Tan, M. K.; Friend, J. R.; Yeo, L. Y. *Phys. Rev. Lett.* **2009**, *103* (2), No. 024501.
(40) Qi, A.; Yeo, L. Y.; Friend, J. R. *Phys. Fluids* **2008**, *20* (7), 074103.
(41) Winkler, A.; Harazim, S. M.; Menzel, S. B.; Schmidt, H. *Lab Chip* **2015**, *15* (18), 3793−3799.
(42) Ding, X.; Peng, Z.; Lin, S.-C. S.; Geri, M.; Li, S.; Li, P.; Chen, Y.; Dao, M.; Suresh, S.; Huang, T. J. *Proc. Natl. Acad. Sci. U. S. A.* **2014**, *111* (36), 12992−12997.
(43) Li, P.; Mao, Z.; Peng, Z.; Zhou, L.; Chen, Y.; Huang, P.-H.; Truica, C. I.; Drabick, J. J.; El-Deiry, W. S.; Dao, M.; Suresh, S.; Huang, T. J. *Proc. Natl. Acad. Sci. U. S. A.* **2015**, *112* (16), 4970−4975.
(44) Destgeer, G.; Ha, B. H.; Park, J.; Jung, J. H.; Alazzam, A.; Sung, H. J. *Anal. Chem.* **2015**, *87* (9), 4627−4632.
(45) Behrens, J.; Langelier, S.; Rezk, A. R.; Lindner, G.; Yeo, L. Y.; Friend, J. R. *Lab Chip* **2015**, *15* (1), 43−46.
(46) Guo, F.; Mao, Z.; Chen, Y.; Xie, Z.; Lata, J. P.; Li, P.; Ren, L.; Liu, J.; Yang, J.; Dao, M.; Suresh, S.; Huang, T. J. *Proc. Natl. Acad. Sci. U. S. A.* **2016**, *113* (6), 1522−1527.
(47) Collins, D. J.; Devendran, C.; Ma, Z.; Ng, J. W.; Neild, A.; Ai, Y. *Sci. Adv.* **2016**, *2* (7), e1600089.
(48) Yeo, L.; Rezk, A. *J. Microelectron. Electron. Compon. Mater.* **2016**, *46* (4), 176−182 (http://www.midem-drustvo.si/Journal%20papers/MIDEM_46(2016)4p176.pdf).
(49) Kabir, K. M. M.; Sabri, Y. M.; Kandjani, A. E.; Matthews, G. I.; Field, M.; Jones, L. A.; Nafady, A.; Ippolito, S. J.; Bhargava, S. K. *Langmuir* **2015**, *31* (30), 8519−8529.
(50) Qi, A.; Friend, J. R.; Yeo, L. Y.; Morton, D. A. V.; McIntosh, M. P.; Spiccia, L. *Lab Chip* **2009**, *9* (15), 2184−2193.
(51) Rezk, A. R.; Tan, J. K.; Yeo, L. Y. *Adv. Mater.* **2016**, *28* (10), 1970−1975.
(52) Fineberg, S. E. *Expert Opin. Invest. Drugs* **2006**, *15* (7), 743−762.
(53) Nuffer, W.; Trujillo, J. *Pharmacol. Pharm.* **2016**, *7* (4), No. 65683.
(54) Martin, M. N.; Basham, J. I.; Chando, P.; Eah, S.-K. *Langmuir* **2010**, *26* (10), 7410−7417.
(55) Sauerbrey, G. *Eur. Phys. J. A* **1959**, *155* (2), 206−222.
(56) Newman, S. P.; Clarke, S. W. *Thorax* **1983**, *38* (12), 881−886.
(57) Alvarez, M.; Friend, J.; Yeo, L. Y. *Nanotechnology* **2008**, *19* (45), 455103.
(58) Patton, J. S.; Bukar, J. G.; Eldon, M. A. *Clin. Pharmacokinet.* **2004**, *43* (12), 781−801.
(59) Profit, L. *Core Evid.* **2005**, *1* (2), 89−101.
(60) Rave, K.; Bott, S.; Heinemann, L.; Sha, S.; Becker, R. H. A.; Willavize, S. A.; Heise, T. *Diabetes Care* **2005**, *28* (5), 1077−1082.
(61) Rashid, J.; Absar, S.; Nahar, K.; Gupta, N.; Ahsan, F. *Expert Opin. Drug Delivery* **2015**, *12* (6), 917−928.
(62) Klonoff, D. C. *J. Diabetes Sci. Technol.* **2014**, *8* (6), 1071−1073.
(63) Nuffer, W.; Trujillo, J. M.; Ellis, S. L. *Ann. Pharmacother.* **2015**, *49* (1), 99−106.
(64) Yeo, L. Y.; Friend, J. R.; McIntosh, M. P.; Meeusen, E. N. T.; Morton, D. A. V. *Expert Opin. Drug Delivery* **2010**, *7* (6), 663−679.
(65) Cortez-Jugo, C.; Qi, A.; Rajapaksa, A.; Friend, J. R.; Yeo, L. Y. *Biomicrofluidics* **2015**, *9* (5), 052603.
(66) Collignon, S.; Manor, O.; Friend, J. *Adv. Funct. Mater.* **2018**, *28* (8), 1704359.

DOI: 10.1021/acs.analchem.8b00466
Anal. Chem. 2018, 90, 5335−5342